Link-Adaptable Vector-Perturbation ZFBF Precoder for Multi-Point 3D-Beamformers

Masaaki Fujii
Samsung R&D Institute Japan
Yokohama, Japan
m.fujii@samsung.com

Abstract—**A link adaptation scheme is devised for vector-perturbation (VP) zero-forcing beamforming (ZFBF) MIMO precoding and a link-adaptable VP-ZFBF precoder is applied to multi-point three-dimensional (3D) beamformers to be used in mmWave-band wireless access systems. Channel coding schemes used in current systems, e.g., turbo codes, possess systematic code structures. The perturbation gain can thus be predicted by searching for perturbation vectors for the symbol vectors mapped from information bits. On the basis of this principle, we constructed an efficient iterative modulation-and-coding-set (MCS) selection procedure for VP-ZFBF precoding. Simulation results demonstrate that our proposed scheme suitably passed on the perturbation gain to the selection of higher MCS and thus achieved high throughputs by incorporating with multi-point 3D-beamformers.**

Keywords—antenna array; 3D-beamforming; MIMO; zero-forcing beamforming; vector perturbation; link adaptation

I. INTRODUCTION

The explosive growth of mobile data traffic is leading to demand for large-capacity mobile communication systems. This demand has recently spurred the development of gigabit-class wireless transmission systems. Such high-rate transmission can be supported by using wideband signals accommodated in high carrier frequencies, e.g., quasi-millimeter wave bands. MmWave bands, however, suffer from large propagation losses. High-gain beamforming techniques afforded by massive antenna arrays are therefore key enablers to the practical use of mmWave bands in cellular systems [1].

Analog-digital hybrid beamformers for massive antenna arrays have been investigated for uplink [2] and downlink [3] as practical configurations. To increase average throughputs, many high-gain beamformers need to be densely deployed around user areas so that sufficient received signal power can be secured at users and multiple streams can arrive at users from different directions. By doing this, both high-order spatial multiplexing and high-rate modulation and coding sets (MCS) are expected to become available to achieve high spectrum efficiency.

Zero-forcing beamforming (ZFBF) is well known as a linear MIMO precoding technique based on channel inversion [4]. It, however, suffers from degradation due to channel correlation. To reduce the degradation, a vector perturbation (VP) technique is applied to ZFBF precoding to significantly improve the transmit power efficiency [5]. In fact, the improvement of throughputs was demonstrated by field experiments [6], but they were limited to fixed MCS. To fully utilize vector-perturbation gain as throughput improvements, link adaptation is a key to the applicability of VP-ZFBF precoding to practical systems. The vector-perturbation gain, however, depends on not only instantaneous channels but also data, modulation orders, perturbation variables, and perturbation vector search parameters. The exact gain is thus determined after the perturbation vector search for channel-coded and modulation-mapped symbol vectors. This makes it difficult to apply channel-adapted MCS selection to VP-ZFBF precoding.

In light of this background, we propose an efficient iterative link adaptation scheme based on systematic code structures. When channel coding is done by using systematic codes such as turbo codes or low-density parity check codes, information bits and parity bits can be separately mapped onto modulation symbols. Starting from MCS selection based on conventional ZFBF precoding, the MCS index is incremented step by step through perturbation-vector search for the symbol vectors mapped from an initial information bit sequence and then extended information bit sequences. We applied our proposed scheme to multi-point three-dimensional (3D) beamformers and evaluated throughout performances. Simulation results demonstrate that the proposed scheme achieved higher throughputs than conventional ZFBF precoding.

II. SYSTEM MODEL

A. Multi-Point 3D-Beamformers

Multiple antenna ports equipped with N_A-element planar arrays are de-centrally deployed in cells as shown in Fig. 1. The number of antenna ports is denoted as M_T. This deployment is regarded as a generalized distributed antenna system (GDAS) or large-scale coordinate multi-point (CoMP). In this system, a link budget is secured from an antenna subset that provides a user with small path losses. The subset size is set to N_T ($\leq M_T$). Moreover, the streams transmitted from distributed antenna ports arrive at a user from different arrival

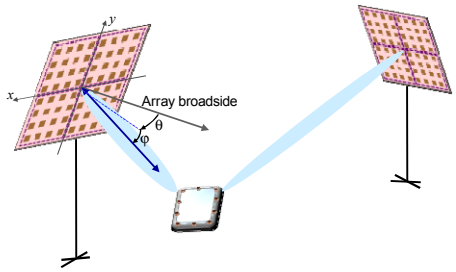

Fig. 1 Multi-point 3D-beamforming.

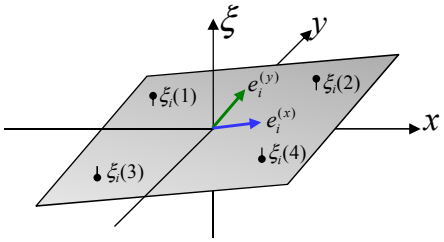

Fig. 2 Phase shift quadratic plane.

angles. The channel matrix is thus more likely to have higher ranks than the one provided with multiple streams transmitted from a single antenna port. The planar array elements are horizontally and vertically partitioned into N_{SA} (= 2×2) subarrays for the sake of directivity control [7]. The N_A-dimensional phased-array weight vector steered to azimuth and elevation angles (θ_i, φ_i) at frame i at antenna port m is expressed as

$$\boldsymbol{b}_i(m) = \frac{1}{\sqrt{N_A}}\left[\exp\{jd_i(1)\}, \quad \cdots, \quad \exp\{jd_i(N_A)\}\right]^T, \tag{1}$$

where $d_i(n_A)$ is the phase delay to be set at antenna element n_A and is given by

$$d_i(n_A) = -\frac{2\pi}{\lambda}\left(p_{n_A}^{(x)} \sin\theta_i \cos\varphi_i + p_{n_A}^{(y)} \sin\varphi_i\right), \tag{2}$$

where $(p_{n_A}^{(x)}, p_{n_A}^{(y)})$ are positions of antenna element n_A, (θ_i, φ_i) are directions to be steered at elevation and azimuth relative to the broadside of the array, and λ is a wavelength. For the initial setting, one of the N_A orthogonal fixed beam directions that provide the largest array-output signal power is chosen in the uplink. Assuming an L-path model, the L-dimensional subarray-output channel response vectors are estimated, and this is denoted $\hat{\boldsymbol{q}}_i(n)$ for subarray n. The array reference vector is then generated by combing N_{SA} response vectors as

$$\hat{\boldsymbol{q}}_i = \frac{1}{N_{SA}} \sum_{n=1}^{N_{SA}} \hat{\boldsymbol{q}}_i(n). \tag{3}$$

The subarray-output channel response vector is correlated with the array reference vector over L paths:

$$\rho_i(n) = \frac{1}{L}\hat{\boldsymbol{q}}_i^T(n)\hat{\boldsymbol{q}}_i^* = \frac{1}{L}\sum_{l=0}^{L-1} \hat{q}_i(l)\hat{q}_i^*(l). \tag{4}$$

The obtained correlation value is normalized to $\overline{\rho}_i(n)$ with unit power, and the phase shift relative to the array center is extracted as shown in Fig. 2 as

$$\xi_i(n) = \mathrm{Im}\{\overline{\rho}_i(n)\}. \tag{5}$$

The slope vector of the quadratic least-squares-error plane is estimated by using $\boldsymbol{\xi}_i = [\xi_i(1), \cdots, \xi_i(N_{SA})]^T$ and an N_{SA} ×2 coordinate matrix $\boldsymbol{A}$ of subarray centers as

$$\boldsymbol{e}_i = \left[e_i^{(x)} \; e_i^{(y)}\right]^T = (\boldsymbol{A}^T\boldsymbol{A})^{-1}\boldsymbol{A}^T\boldsymbol{\xi}_i, \tag{6}$$

where the entries of $\boldsymbol{A}$ are given for subarray n by

$$\left\{a_x(n), a_y(n)\right\} = \left\{\frac{1}{N_\Lambda}\sum_{n_A \in \Lambda_n}\frac{p_{n_A}^{(x)}}{\lambda}, \frac{1}{N_\Lambda}\sum_{n_A \in \Lambda_n}\frac{p_{n_A}^{(y)}}{\lambda}\right\}, \tag{7}$$

where Λ_n is an antenna element subset for subarray n and N_Λ is the subset size. The directivity control errors are estimated by transforming $\boldsymbol{e}_i$ as

$$\left(\Delta\hat{\theta}_i, \Delta\hat{\varphi}_i\right) = \left(e_i^{(x)}/2\pi\cos\theta_i, \; e_i^{(y)}/2\pi\cos\varphi_i\right). \tag{8}$$

The beam directions are updated by using a step size parameter μ as

$$(\theta_{i+1}, \varphi_{i+1}) = (\theta_i, \varphi_i) + \mu\left(\Delta\hat{\theta}_i, \Delta\hat{\varphi}_i\right). \tag{9}$$

The phased-array steering vector is updated to $\boldsymbol{b}_{i+1}(m)$. Let $\boldsymbol{H}(m)$ be an N_R×N_A downlink channel matrix between N_R receive antennas and N_A antenna elements. The effective channel vector is then generated as $\boldsymbol{g}(m) = \boldsymbol{H}(m)\boldsymbol{b}_F(m)$ at frame $i = F$ between the user and antenna port m. The N_R×N_T effective downlink channel matrix is therefore denoted as $\boldsymbol{G} = [\boldsymbol{g}(1) \;\; \boldsymbol{g}(2) \;\; \cdots \;\; \boldsymbol{g}(N_T)]$.

B. Applicability of Vector-Perturbation MIMO Precoding

The wireless links between N_R receive antennas and N_T beamformers are regarded as N_R×N_T MIMO channels. The inter-stream interferences are preferably rejected at the transmitter side to curtail the power consumption at the user equipment. For this end, MIMO precoding techniques can be applied to the symbol vectors to be transmitted. A VP technique is well known as a way of improving the transmission performance of linear precoding techniques such as ZFBF precoding. Considering link adaptation, the interdependent relationship between MCS selection and perturbation vector (PV) search makes it difficult to select an adequate MCS as illustrated in Fig. 3. The VP gain needs to be estimated prior to MCS selection to reflect the VP gain to the selection of a higher-rate MCS. The gain is, however, determined after the PV search for channel-coded and modulation-mapped symbol vectors specified by an MCS index. This is the so-called chicken-or-the-egg problem. In addition, the exact VP gain depends on a ZFBF matrix, a coded bit sequence, modulation orders, perturbation variables, and perturbation vector search parameters. The theoretical

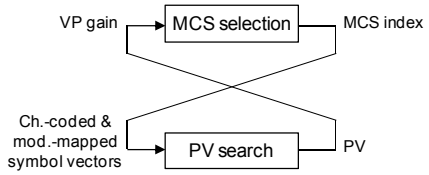

Fig. 3 Interdependent relationship between MCS selection and PV search.

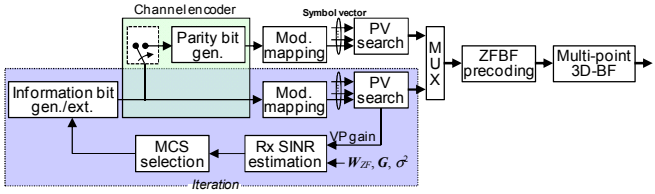

Fig. 4 Transmitter configuration.

derivation of the exact VP gain is thus considered unfeasible. A clue to resolve this issue that we found is as follows. First, information bits and parity bits are separately mapped onto modulation constellations on the basis of systematic code structures to separate the selection of coding rates and modulation orders. Secondly, MCS selection and PV search are alternately carried out in an iterative fashion to acquire larger VP gain with use of higher-order modulations. The details of the MCS selection procedure that we developed are described in the subsequent section.

III. Iterative MCS Selection Based on Systematic Code Structure

Figure 4 shows a transmitter configuration including the MCS selection that we propose. Figure 5 shows a procedure example of generating link-adapted vector-perturbation symbol vectors by updating an MCS index. The overall procedure is described as follows.

Step 1: *Tentative MCS Selection Based on ZFBF Precoding*

The weight matrix of ZFBF precoding is given by $\boldsymbol{W}_{ZF} = \boldsymbol{G}^{-1}$. The signal vector to be transmitted is assumed to be

$$\boldsymbol{z}(k) = \sqrt{\frac{P}{\gamma_{ZF}}}\boldsymbol{W}_{ZF}\boldsymbol{s}(k), \tag{10}$$

where P is the transmit power, $\boldsymbol{s}(k)$ is the symbol vector to be transmitted at symbol index k, and γ_{ZF} is a normalization factor. The normalization factor is given by

$$\begin{aligned}\gamma_{ZF} &= E\left\|\boldsymbol{W}_{ZF}\boldsymbol{s}(k)\right\|^2 \\ &= \left\|\boldsymbol{W}_{ZF}\right\|_F^2,\end{aligned} \tag{11}$$

where $E[\|\boldsymbol{s}(k)\|^2] = 1$ was used and $\|\cdot\|_F$ is the Frobenius norm. The received signal vector is assumed to be

$$\boldsymbol{y}(k) = \boldsymbol{G}\boldsymbol{z}(k) + \boldsymbol{n}(k) = \sqrt{\frac{P}{\gamma_{ZF}}}\boldsymbol{s}(k) + \boldsymbol{n}(k), \tag{12}$$

where $\boldsymbol{n}(k)$ is a noise vector with a variance of σ^2 for each entry. The SINR is estimated as

$$SINR_{ZF} = 10\log_{10}\frac{P}{\gamma_{ZF}\sigma^2}. \tag{13}$$

An MCS index is tentatively selected on the basis of the estimated SINR by referring to an MCS table. The selected MCS index specifies modulation order M, coding rate R, and information bit length N_i (Fig. 5(a)).

Step 2: *Modulation Mapping and Perturbation Vector Search*

The information bits with length N_i in N_T streams are mapped on modulation symbol vector $\boldsymbol{s}_M(k)$ with modulation order M and with symbol length N_s (Fig. 5(b)). Perturbation vectors (PV) are then searched for in such a way that the squared norm of the precoded signal vector can be minimized as

$$\boldsymbol{l}(k) = \arg\min_{\boldsymbol{l}'}\left\|\boldsymbol{W}_{ZF}\left\{\boldsymbol{s}_M(k) + \tau_M\boldsymbol{l}'\right\}\right\|^2, \tag{14}$$

where τ_M is a perturbation interval for modulation order M and $\boldsymbol{l}'$ is perturbation-vector candidates (Fig. 5(c)). The perturbation interval of the constellation is chosen as $\tau_M = 2\beta_M(|c_{\max}| + \Delta/2)$, where $|c_{\max}|$ is the absolute value of the constellation symbols with largest magnitude, Δ is the spacing between constellation points, and β_M is an enlargement factor for modulation order M that provides a trade-off between the reduction of modulo arithmetic errors and the perturbation gain [8]. The larger the modulation order M, the smaller the optimum enlargement factor β_M. As a result, the larger the modulation order used, the larger the vector-perturbation gain that tends to be provided. This incremental gain for higher order modulations therefore needs to be reflected in the MCS selection. The entry of $\boldsymbol{l}'$ has N_V candidates of perturbation variables. The number of perturbation vector candidates is thus $N_V^{N_T}$. This becomes enormous for practical sizes N_V and N_T. Therefore, the perturbation vector is efficiently searched for by using QR-decomposition of $\boldsymbol{W}_{ZF}$ and M-algorithm [9]. Here we use sorted QR-decomposition to more efficiently search for the perturbation vector $\boldsymbol{l}(k)$.

Step 3: *MCS Update, Modulation Mapping, and Pertrubation Vector Search*

The signal vector to be transmitted is assumed to be

$$\boldsymbol{z}(k) = \sqrt{\frac{P}{\gamma_{VP}(M)}}\boldsymbol{W}_{ZF}\left\{\boldsymbol{s}_M(k) + \tau_M\boldsymbol{l}(k)\right\}, \tag{15}$$

where $\gamma_{VP}(M)$ is a normalization factor and is calculated as

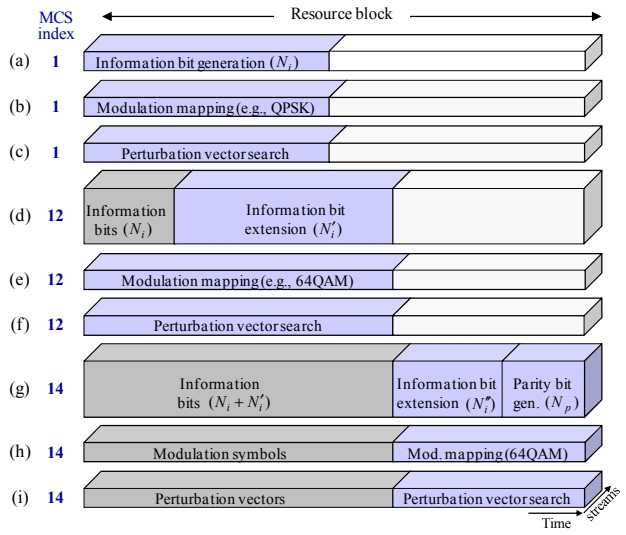

Fig. 5 A procedure example of updating an MCS index and generating vector-perturbation symbol vectors.

$$\gamma_{VP}(M) = \frac{1}{N_s} \sum_{k=1}^{N_s} \left\| \boldsymbol{W}_{ZF} \{ \boldsymbol{s}_M(k) + \tau_M \boldsymbol{l}(k) \} \right\|^2 . \quad (16)$$

When the perturbation-vector candidates include the zero vector corresponding to ZFBF precoding (no perturbation), $\gamma_{VP}(M) \le \gamma_{ZF}$ is guaranteed. The improved SINR is estimated as

$$SINR_{VP}(M) = 10 \log_{10} \frac{P}{\gamma_{VP}(M) \sigma^2} . \quad (17)$$

When $SINR_{VP}(M)$ is below the required SNR of the highest coding rate prepared for modulation order M, the subsequent Step 4 will be carried out by setting $M' = M$ and $R' = R$.

When $SINR_{VP}(M)$ exceeds the required SNR of the highest coding rate prepared for modulation order M, the MCS index is updated by referring to the MCS table as $M \to M'$ and $R \to R'$. The information bits are extended by length N_i' (Fig. 5(d)) and then mapped onto modulation symbols (Fig. 5(e)). The perturbation vectors are newly searched for (Fig. 5(f)) as

$$\boldsymbol{l}(k) = \arg \min_{\boldsymbol{l}'} \left\| \boldsymbol{W}_{ZF} \{ \boldsymbol{s}_{M'}(k) + \tau_{M'} \boldsymbol{l}' \} \right\|^2 . \quad (18)$$

The normalization factor is re-calculated as

$$\gamma_{VP}(M') = \frac{1}{N_s'} \sum_{k=1}^{N_s'} \left\| \boldsymbol{W}_{ZF} \{ \boldsymbol{s}_{M'}(k) + \tau_{M'} \boldsymbol{l}(k) \} \right\|^2 , \quad (19)$$

where N_s' is the symbol length determined by information bit length $N_i + N_i'$ and modulation order M'. By increasing the modulation order, $\gamma_{VP}(M')$ is likely to be smaller than $\gamma_{VP}(M)$. The SINR is updated as $SINR_{VP}(M')$ and its incremental gain is transformed into the selection of higher coding rates in Step 4.

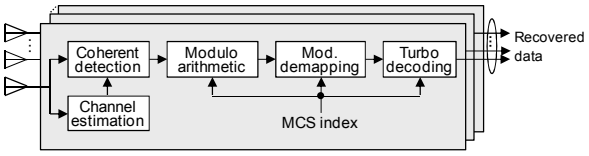

Fig. 6 Receiver configuration.

Step 4: *Coding Rate Update, Parity Bit Generation, Modulation Mapping, and Perturbation Vector Search*

When $SINR_{VP}(M')$ exceeds the required SNR of the coding rate selected at present, the coding rate is updated as $R' \to R''$. Note that even if $SINR_{VP}(M')$ exceeds the selection boundary of the modulation order, the modulation order will not be further updated so as to keep the complexity low by allowing a small loss due to the selection of a lower MCS index. The information bits are extended by length N_i''. The information bits with total length $N_i + N_i' + N_i''$ are fed into the channel encoder to calculate parity bits with length N_p (Fig. 5(g)). The extended information bits and parity bits are mapped on modulation symbols (Fig. 5(h)). The perturbation vectors for these symbol vectors are then searched for (Fig. 5(i)) as

$$\boldsymbol{l}(k) = \arg \min_{\boldsymbol{l}'} \left\| \boldsymbol{W}_{ZF} \{ \boldsymbol{s}_{M'}(k) + \tau_{M'} \boldsymbol{l}' \} \right\|^2 . \quad (20)$$

The transmit power normalization factor is re-calculated as

$$\gamma_{VP}'(M') = \frac{1}{N_s''} \sum_{k=1}^{N_s''} \left\| \boldsymbol{W}_{ZF} \{ \boldsymbol{s}_{M'}(k) + \tau_{M'} \boldsymbol{l}(k) \} \right\|^2 , \quad (21)$$

where N_S'' is the symbol length of the resource block. The summation of up to N_s' is already calculated in (19) and thus is utilized for simplicity. The VP-ZFBF-precoded symbol vectors are generated as

$$\boldsymbol{z}(k) = \sqrt{\frac{P}{\gamma_{VP}'(M')}} \boldsymbol{W}_{ZF} \{ \boldsymbol{s}_{M'}(k) + \tau_{M'} \boldsymbol{l}(k) \} . \quad (22)$$

The VP-ZFBF-precoded symbol vector is sent to the multi-point 3D-beamformers.

IV. Receiver Structure

Figure 6 shows a receiver configuration. The N_R-dimensional received signal vector is given by

$$\begin{aligned} \boldsymbol{y}(k) &= \boldsymbol{G}\boldsymbol{z}(k) + \boldsymbol{n}(k) \\ &= \sqrt{\frac{P}{\gamma_{VP}'(M')}} \boldsymbol{G}\boldsymbol{W}_{ZF} \{ \boldsymbol{s}_{M'}(k) + \tau_{M'} \boldsymbol{l}(k) \} + \boldsymbol{n}(k) \\ &= \sqrt{\frac{P}{\gamma_{VP}'(M')}} \{ \boldsymbol{s}_{M'}(k) + \tau_{M'} \boldsymbol{l}(k) \} + \boldsymbol{n}(k) , \end{aligned} \quad (23)$$

where $\boldsymbol{G}\boldsymbol{W}_{ZF} = \boldsymbol{I}$ was used. At each Rx antenna branch, the received signals are coherently detected. The coherently

detected signal vector is normalized by the VP gain and then the modulo operation is then carried out as

$$\tilde{\boldsymbol{y}}(k) = \boldsymbol{s}_{M'}(k) + \boldsymbol{n}'(k) \ , \tag{24}$$

where

$$\boldsymbol{n}'(k) = \frac{\boldsymbol{n}(k)}{\sqrt{\frac{P}{\gamma'_{VP}(M')}}} \ . \tag{25}$$

After that, the recovered symbols are de-mapped into bit-by-bit log-likelihood ratios and are then fed into the turbo decoder to recover the data. Here the feedback of $\boldsymbol{G}$ to the antenna ports is assumed to be perfect. Therefore, the inter-stream interference is assumed to be negligible.

V. Computer Simulation

The throughput performances of the proposed scheme were evaluated under various conditions. Table I lists the simulation parameters and Table II lists the MCS table in which the indexes are arranged in ascending order of the spectrum efficiencies, that is, the required SNRs.

TABLE I. Simulation Parameters

Transmit Signals	
Resource block size	480 symbols
Channel coding	Turbo codes
Modulation mapping	Separation mapping for information bits and parity bits
Perturbation variables	0, ±1, ±j1, ±1±j1 (N_V = 9)
Enlargement factor for perturbation intervals	1.5 (QPSK), 1.4 (16QAM), 1.3 (64QAM), 1.2 (256QAM)
Number of survivor paths in M-algorithm	81
Target packet error rate	1.0×10^{-3}
Antenna Arrays	
Antenna tilt	6.8 deg.
Array size	N_A = 64, 144, and 256
Inter-element distance	$D_x = 0.55\lambda$ and $D_y = 0.7\lambda$
Step size parameter in directivity control	μ = 0.1
Channel Model	
Carrier frequency	28 GHz
Antenna port deployment	Circular-layout GDAS model h = 6 m, r_c = 50 m, r_u = 40 m
Number of antenna ports deployed in cell	M_T = 12
Number of antenna ports used for transmission	N_T = 10
Path loss exponent	3.4
Shadowing deviation	9.8 dB
Path model	1-path 3D channel model (32 sub-paths)
Path angle deviation (azimuth, elevation)	$\sigma_{\delta,\,BF}$ = (0.0, 0.0) deg. $\sigma_{\delta,\,user}$ = (10.0, 10.0) deg.
Sub-path offset deviation (azimuth, elevation)	$\sigma_{\Delta,\,BF}$ = (1.0, 1.0) deg. $\sigma_{\Delta,\,user}$ = (5.0, 5.0) deg.
Average SNR at center point (w/o array gain)	0.7 dB
Receiver	
Number of Rx antennas	N_R = 10 (deployed on A4 note size)
Turbo decoding	Max-log-MAP decoding with 8 iterations
Channel estimation	Ideal at both Tx and Rx

TABLE II. MCS Table

Index	Modulation	Rate	Index	Modulation	Rate
1	QPSK	1/2	11	16QAM	8/9
2	QPSK	2/3	12	64QAM	2/3
3	QPSK	3/4	13	64QAM	3/4
4	QPSK	4/5	14	64QAM	5/6
5	QPSK	6/7	15	64QAM	8/9
6	QPSK	8/9	16	256QAM	3/4
7	16QAM	2/3	17	256QAM	4/5
8	16QAM	3/4	18	256QAM	5/6
9	16QAM	4/5	19	256QAM	6/7
10	16QAM	6/7	20	256QAM	8/9

In the MCS table, 256QAM is included to evaluate potential capabilities although the application of the vector perturbation to 256QAM may not be practical. We used a circular-layout GDAS model [10] as antenna port deployment and user distribution as shown in Fig. 7. We referred to [11] to set up some NLOS parameters. The one path model in the resource block corresponds to, e.g., a frequency-domain one-tap channel response in OFDM signals. The channel vector $\hat{\boldsymbol{q}}_i(n)$ in (3) and (4) was thus reduced to a scalar value because of L = 1. The channels are assumed to be invariant within the resource block. Throughout the computer simulations, the average packet error rates at the receiver were around 1.0×10^{-3} as targeted.

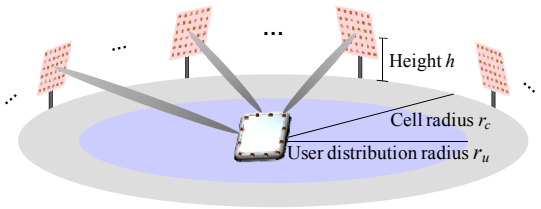

Fig. 7 Circular-layout GDAS model.

A. Effect of 3D-Beamsteering

Figure 8 plots the cumulative distribution function (CDF) of the throughputs provided with the VP-ZFBF precoding when N_A = 256. The dashed lines indicate the throughputs when one of the fixed beams was selected and used. The number of fixed beams used in the simulation set-up was only N_A and nearly half of them were not used because the user was assumed to be located on the ground and thus the array gain was not fully utilized when the user was located off the beam directions. Starting from the selected beam directions, the beam directivity was controlled on the basis of the proposed directivity control scheme in uplink. The number of frames used for the directivity control update was F = 20. The resultant steered beams were used for the downlink transmission. As shown in the solid line, the throughputs were significantly improved from those provided with the fixed beams because larger array gains were provided to the user.

In addition, the throughputs provided with the directivity control were close to those obtained by the ideal beam pointing (plotted in the dotted line) in which the antenna ports hypothetically know the user direction. This is because the

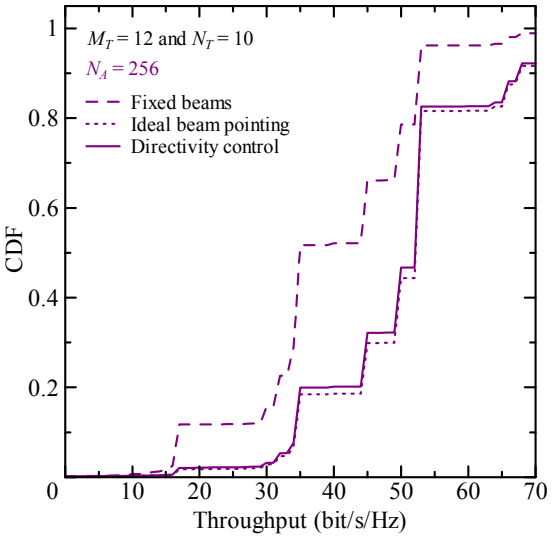

Fig. 8 Effect of 3D-beamsteering on throughputs.

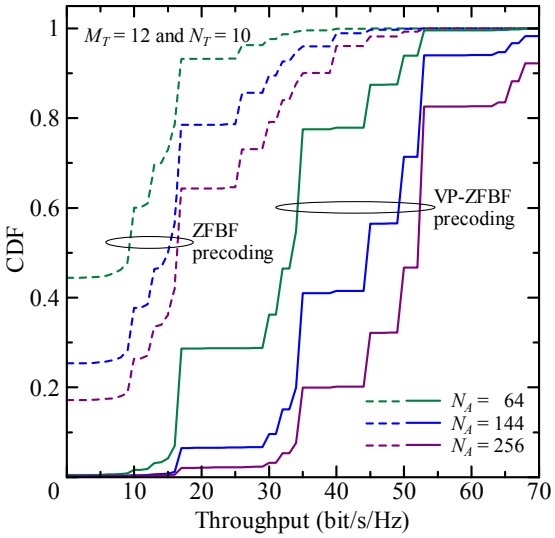

Fig. 9 Throughput comparison between ZFBF precoding and VP-ZFBF precoding.

SINR was quantized to 20 levels of MCS even if there was a small gap between SINRs provided with the directivity control and the ideal beam pointing.

B. Throughput Comparison with ZFBF Precoding

Figure 9 plots the CDF of the throughputs for N_A = 64, 144, and 256. As the array size increased, the throughputs increased because of larger array gains for both the ZFBF precoding and the VP-ZFBF precoding. As shown in the graph, the VP-ZFBF precoding significantly improved the throughput performances provided with the ZFBF precoding because of the improved transmit power efficiency. By setting $N_A = 256$, the throughputs at CDF = 0.5 were over 50 bit/s/Hz.

It is worth mentioning that the CDF lines of the VP-ZFBF precoding exhibited *walls* at 17.8, 35.6 and 53.3 bit/s/Hz in Fig. 9. These rates correspond to the highest coding rate used in each modulation order. These walls occurred for a way to keep the complexity low as described in Step 4.

VI. Conclusion

We proposed a link-adaptable VP-ZFBF precoder and applied it to multi-point 3D beamformers. The iterative MCS selection scheme based on systematic code structures efficiently selected modulation orders and coding rates to sufficiently utilize instantaneous channel conditions and vector perturbation gain. In addition, the throughputs over 50 bit/s/Hz were achieved with the CDF of 50% when 10 antenna ports were dynamically selected out of 12 fixed antenna ports equipped with 256-element 3D-beamformers, which were deployed in the circular-layout GDAS model. Our proposed scheme will therefore contribute to increasing throughputs and achieving several ten gigabit/s assuming approximately several hundred MHz ~ 1 GHz signal bandwidth at mmWave bands.

References

[1] W. Roh, J. Seol, J. Park, B. Lee, J. Lee, Y. Kim, J. Cho, K. Cheun, and F. Aryanfar, “Millimeter-wave beamforming as an enabling technology for 5G cellular communications: theoretical feasibility and prototype results,” IEEE Communications Magazine, vol.52, no.2, pp.106-113, February 2014.

[2] M. Fujii, J. Seol, T. Kim, and J. Cho, “Subarray-processing iterative SISO multi-user detection and multi-beam directivity control for large-scale antenna array,” ISPACS2013, Okinawa, Japan, November 2013.

[3] T. Obara, S. Suyama, J. Shen, and Y. Okumura, “Joint fixed beamforming and eigenmode precoding for super high bit rate massive MIMO systems using higher frequency bands,” PIMRC2014, Washington, DC, USA, September 2014.

[4] B.M. Hochwald, C.B. Peel, and A.L. Swindlehurst, “A vector-perturbation technique for near-capacity multiantenna multiuser communication − part I: channel inversion and regularization,” IEEE Trans. Commun., vol.53, no.1 pp.195-202, January 2005.

[5] B.M. Hochwald, C.B. Peel, and A.L. Swindlehurst, “A vector-perturbation technique for near-capacity multiantenna multiuser communication − part II: perturbation,” IEEE Trans. Commun., vol.53, no.3 pp.537-544, March 2005.

[6] S. Sonobe, S. Tsukamoto, T. Maeda, K. Yano, H. Ban, M. Uno, and K. Kobayashi, “Field experiments of LTE-Advanced-based 8×8 multiuser MIMO system with vector perturbation,” WiNMee2013, Tsukuba Science City, Japan, pp.83-88, May 2013.

[7] M. Fujii, J. Seol, T. Kim, and J. Cho, “Performance comparison between single- and multiple-arrays for 3D-beamsteering multi-user detection,” GCCE2014, Makuhari Messe, Tokyo, Japan, October 2014.

[8] H. Mori, Y. Tohzaka, T. Aoki, and Y. Tanabe, “Throughput improvement technique using adaptive control of perturbation interval for downlink multi-user MIMO based on vector perturbation,” IEICE Trans. Commun., vol.E95-B, no.9, pp.2861-2869, September 2012.

[9] M. Mohaisen, B. Hui, K. Chang, S. Ji, and J. Joung, “Fixed-complexity vector perturbation with block diagonalization for MU-MIMO systems,” MICC2009, Kuala Lumpur, Malaysia, pp.238-243, December 2009.

[10] X. Wang, P. Zhu, and M. Chen, “Antenna location design for generalized distributed antenna systems,” IEEE Commun. Letters, vol.13, no.5, pp.315-317, May 2009.

[11] M.K. Samimi and T.S. Rappaport, “Ultra-wideband statistical channel model for 28 GHz millimeter-wave urban NLOS environments”, GLOBECOM2014, Austin, TX USA, December 2014.